RSC Advances

ROYAL SOCIETY OF CHEMISTRY

www.rsc.org/advances

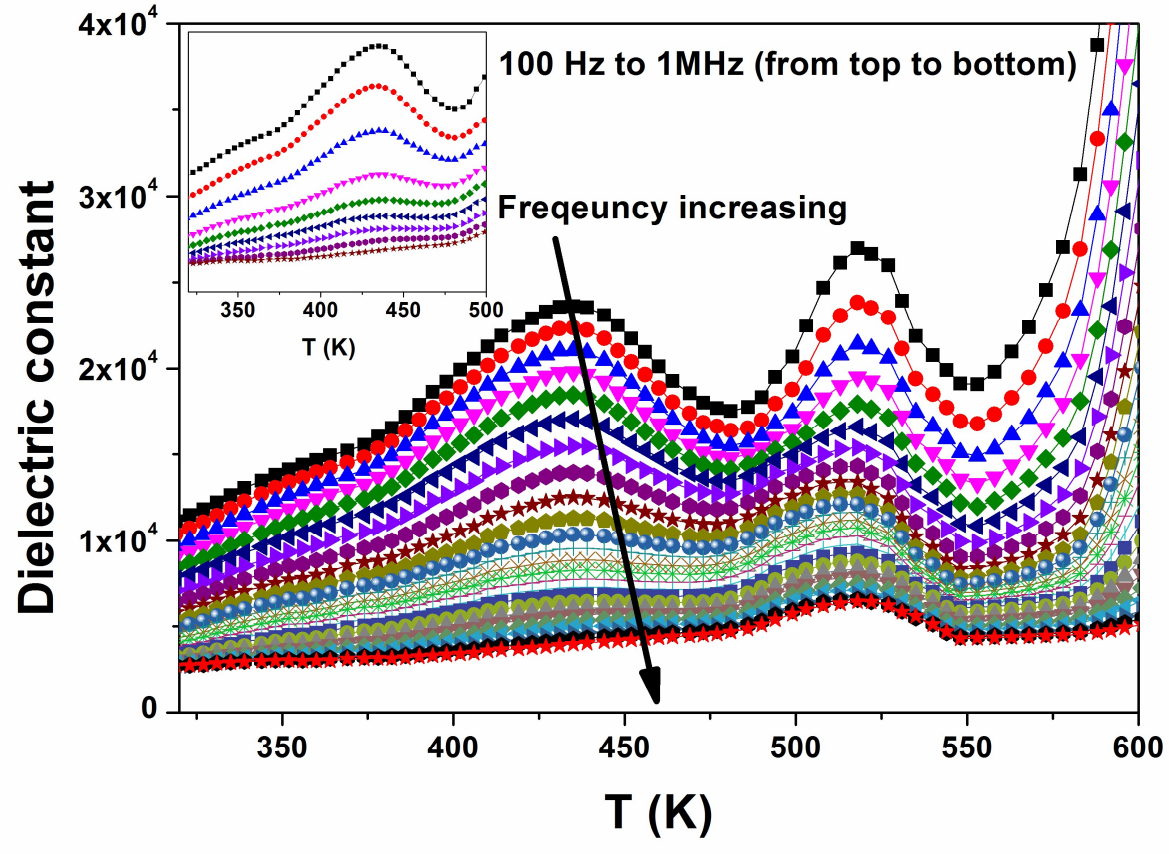

HIGH TEMPERATURE DIELECTRIC RELAXATION ANAMOLIES IN $Ca_{0.9}Nd_{0.1}Ti_{0.9}Al_{0.1}O_{3-\delta}$ SINGLE CRYSTALS

G. Murugesan, R. Nithya[a], S. Kalainathan[*], Shamima Hussain[b],

Centre for Crystal Growth, School of Advanced Sciences, VIT University, Vellore 632 014, Tamil Nadu, India
[a]Materials Science Group, Indira Gandhi Centre for Atomic Research, Kalpakkam 603 102, Tamil Nadu, India
[b]UGC-DAE Consortium for Scientific Research, Kalpakkam Node, Kokilamedu 603104 , India

Abstract

We herein report the dielectric studies on $Ca_{0.9}Nd_{0.1}Ti_{0.9}Al_{0.1}O_{3-\delta}$ single crystals grown by optical floating zone technique in the temperature range from room temperature to 660K. Two dielectric anomalies were observed at ~436K and 520K, which corresponds to relaxor-like behaviour due to Maxwell-Wagner relaxations and conduction relaxation associated with doubly ionized oxygen vacancy respectively. The presence of Ti^{3+} for charge carriers hopping and oxygen vacancy is confirmed by X-ray photo spectroscopy analysis.

INTRODUCTION

Due to its versatile properties $CaTiO_3$ (CTO) has been used as a matrix for storing nuclear waste (SYNROC) [1], high permittivity and low dielectric loss makes it suitable for microwave dielectric applications as resonators and filters [2], it can also be used as host for rare earth ions for efficient luminescence [3]. $CaTiO_3$ is an incipient ferroelectric at low temperatures and doping of Pb up to x=0.3 in $Ca_{1-x}Pb_xTiO_3$ makes it ferroelectric [4-5]. $CaTiO_3$ (orthorhombic) – $NdAlO_3$ (rhombohedral) based ceramics are structurally compatible which allows them to be used for commercial production of microwave dielectric resonators in wireless communications [6].

Recently dielectric anomalies occurring at higher temperatures other than ferroelectric transitions are being reported [7-13]. These anomalies are strongly related to oxygen vacancies and Maxwell-Wagner mechanism which is due to the electrical inhomogeneity in the sample. Oxygen vacancy brings about dielectric relaxation in the material and also it is a key factor to understand many properties like electrical, magnetic and optical properties [7]. Thus interest has been turned out in understanding the vital importance of oxygen vacancy. Few reports on the high temperature dielectric study on single crystals reveal that these anomalies are dielectric relaxations due to oxygen vacancies, dipolar and Maxwell-Wagner mechanisms [7-9]. Bidault et al., [14] have done high temperature dielectric studies on flux grown CTO single crystal, where they found an anomaly at 680^{o}C which was attributed to mono dispersive Debye-type dielectric relaxation due to oxygen vacancies. To our knowledge there are no investigations on high temperature dielectric properties of $Ca_{0.9}Nd_{0.1}Ti_{0.9}Al_{0.1}O_{3-\delta}$ (CNTAO) single crystals. This motivated us to undertake investigations of dielectric properties at high temperatures. In this paper, we present the dielectric properties of CNTAO single crystal in the temperatures ranging from room temperature to 660K.

EXPERIMENTAL

The single crystals of CNTAO were grown by optical floating zone technique in argon atmosphere [15]. Temperature dependence of dielectric response is measured in the heating mode at the rate of 1°C/min from 315K to 660K using N4L PSM1735 (Newton4th Ltd, UK) impedance analyzer in the frequency range of 100 Hz to 1 MHz. Frequency dependence of dielectric measurements were carried out in the frequency range of 50Hz to 5MHz. X-ray photoelectron spectra for as grown crystals were recorded using M/s Specs Spectrometer with a DLSEGD detector with a monochromatic Al K_{α} X-ray source (resolution was 0.1eV at band pass energy of 50eV).

RESULTS AND DISCUSSION

Fig.1 shows the temperature dependence of real part of complex permittivity for CNTAO single crystals in the measured temperature range at various frequencies. It is clear that there are two anomalies occurring ~436K and 520K. The peak position of the low temperature anomaly moves to higher temperature side with decreasing peak intensity as frequency increases proving it to be a relaxor-like behaviour [7-8]. The higher temperature anomaly is frequency independent but its intensity decreases for increasing frequency which is termed as phase-transition-like anomaly [7-8]. The subsequent increase of dielectric constant at higher temperatures is due to the increase of conduction in the sample [14].

In order to understand the nature of dielectric relaxations leading to these anomalies, we performed frequency dependent dielectric permittivity at various temperatures. The frequency dependence of dielectric constant (ε′) and dielectric loss (ε") are shown in Figs. 2 and 3 respectively.

A step like decrease in ε′ with increasing frequency signifies the presence of relaxation in the grown crystal for the low temperature region [16]. The relaxation processes could be analyzed in terms of Debye behaviour or Maxwell-Wagner (MW) behaviour. For a Debye system ε" tends to zero as the frequency reduces to zero, whereas in the MW behaviour ε" tends to infinity as frequency reduces to zero [17]. In our case the later one is applicable. From Fig. 3 it is evident that ε" tends to higher values rather than zero proving it to be a MW relaxation process. The increase of ε" with decreasing frequency indicates it to be a MW effect [17]. MW type relaxation can occur due to the electrical inhomogeneities of the sample or grain boundaries [18]. Our measurements on single crystals eliminate the grain boundary contribution to polarization. The electrode polarization (EP) effect is seen for

lower frequencies, since the charge carriers have enough time at low frequencies to accumulate at the sample-electrode interfaces [19].

Formation of Schottky barriers (layer with depleted charge carriers) at the electrode-sample interface due to the difference in work functions of metal (electrode) and the semiconductor (sample) can also attribute to electrode polarization. In order to determine the conducting nature of the grown crystal, impedance analysis was done. The variation of real part of impedance (Z′) with frequency for various temperatures is shown in Fig. 4. The decrease of Z′ with the increase in temperature in lower frequencies show a negative temperature coefficient of resistance type behaviour similar to that of semiconductors, further the merging of Z′ values for all temperatures at high frequencies may be due to the release of space charge due to the reduction in barrier properties at rise in temperature [20]. This clearly indicates the accumulation of charges at the sample-electrode interface.

The variation of Z" with frequency at different temperatures is shown in Fig. 5. The broadening of peak which is slightly asymmetrical with the rise in temperature suggests that there is a temperature dependent electrical relaxation in grown single crystal of CNTAO [20, 21]. The relaxation time τ is calculated using the relation $2\pi f_p \tau = 1$ (here f_p is the frequency corresponding to maximum Z") from the peak positions of the plot in Figure 5 (Z" vs frequency). The inset in Fig. 5 shows the variation of τ vs. 1000/T, The activation energy is found by linear fit of Arrhenius equation:

$$\tau = \tau_0 e^{\frac{-E_{relax.}}{k_B T}} \quad \text{(1)}$$

where τ_o is the pre-exponential factor, T is the temperature and k_B is the Boltzmann constant.

The deviation in Arrhenius equation at higher temperature clearly shows the presence of another relaxation mechanism at higher temperature. The activation energy for LT region

is found to be 0.40eV and HT region is found to be 1.0eV. In order to understand the physical nature of the relaxations, frequency dependence of tanδ were analyzed in low and high temperature regions. The frequency dependence of tanδ is shown in Fig. 6. The inset in Fig. 6 shows peak position f_p (frequency corresponding to maximum tanδ at a particular temperature) vs. 1000/T. The deviation in Arrhenius equation is clearly seen from low temperature region to higher temperature region. The activation energies calculated for two regions are 0.40eV and 0.83eV respectively. The deviation in Arrhenius equation and presence of different activation energies for different temperature regions is due to the change of relaxation mechanisms [7]. The value of activation energy for the low temperature region is associated with the oxygen vacancies clustering, the energy required to move these clusters is less than the energy required to move individual oxygen vacancies [7, 22 and 23]. Oxygen vacancies can also trap charge carriers, the hopping of trapped charge carriers between trap sites with increase in temperature give rise to dipolar effect [7]. To further probe the relaxation behaviour of low temperature anomaly, the electric moduli was calculated and the plot for M" (T) is shown in Fig. 7. It is clear from the plot that there is a shift in peak temperature for higher temperatures with increasing frequency indicating a thermally activated relaxation [8].

From the Arrhenius law the relaxation parameters are calculated,

$$f = f_0 e^{\frac{-E_{relax.}}{k_B T_p}} \quad \text{(2)}$$

where f_0 is the pre-exponential factor, $E_{relax.}$ is the activation energy for relaxation, k_B is the Boltzmann constant and T_p is the temperature corresponding to the peak maximum in M"(T). The inset of Fig. 7 shows the Arrhenius plot, from which activation energy for relaxation was deduced to be 0.52eV. In order to determine whether these anomalies are related to oxygen

vacancies, the grown crystal was annealed in O_2 atm at 1000^0C for 6hrs. The as grown crystals were black in colour and when annealed it became transparent which is shown as inset in Fig 8. The dielectric property as a function of temperature was done for the annealed sample. Fig. 8 shows the temperature dependence of dielectric constant for pre annealed and post annealed samples. It is clearly seen that the intensity of both anomalies decreases for O_2 annealed samples proving it to be related to oxygen vacancies. Earlier reports have proved that the relaxations similar to LT region is due to the dipolar relaxation (hopping motion of trapped charge carriers) and a MW relaxation due to the blocking of the hopping carriers at the sample/electrode interface [8-9]. The activation energy of high temperature region is compatible with the activation energy of movement of oxygen ions or oxygen vacancies [7, 24]. The high temperature region anomaly is a conduction relaxation due to the movement of doubly ionized oxygen vacancies which will be explained later.

In order to study the electrode polarization effect, we conducted Nyquist plot analysis in order to separate the interfacial effect from the bulk effect. The Nyquist plot (Z" vs. Z′) is shown in Fig.9. It is evident that the decrease in radius of the semicircle with the increase in temperature shows that the resistivity decreases with the temperature. The semicircle in Nyquist plot shows the presence of dielectric relaxation in the crystal with its diameter representing the resistance of the measured sample [25]. Single semicircular arc is present at all temperatures at higher frequency region which is due to the relaxation belonging to bulk dielectric response of the material. The faint tail appearing at low frequency can be ascribed to the dielectric response due to the contact by sample/electrode [25]. Fig. 10 shows the Nyquist plot for CNTAO crystal at 574K, this behaviour is modelled by double layered model consisting of two RC (R- Resistance, CPE- Constant Phase Element) circuits (one for bulk and other one for contact) connected in series as shown in inset of Fig. 10 [26]. The equivalent circuit was fitted by using EIS spectra analyser 1.0 [27]. Due to the electrode

polarization effect, we could not observe a full semi circular arc for all the temperatures. The semicircular arc for the bulk dielectric response is simulated as shown in Fig. 10. The constant phase element is a non ideal frequency dependent capacitance which can be associated with distribution of relaxation times [28-29]. The impedance of CPE is defined as

$$Z_{CPE} = \frac{1}{A(j\omega)^n} \quad \text{(3)}$$

where the CPE is treated as an ideal capacitor for n=1 and resistor for n=0 [26]. Fitted parameters of the equivalent circuit are shown in Table 1. The values of R_1, C_1 & n_1 correspond to dielectric response due to the electrode/sample interface and the values of R_2, C_2 & n_2 correspond to the bulk response of the material. The n_2 value is about 0.978 (close to 1) which shows that the CPE for the bulk dielectric response can be treated as an ideal capacitor.

Fig. 11 shows the spectroscopic plots of M" at various temperatures. The positions of the modulus peaks shift to higher frequencies with the increasing temperature, which shows the presence of thermally activated relaxation in the CNTAO crystal [25].

The high temperature dielectric anomalies in oxides is due to the oxygen vacancies, the activation energy value lies between 0.3-1.0eV for the relaxations caused by oxygen vacancies [8]. To prove that these anomalies in single crystal sample are related to delocalized carriers, we performed analysis on the conduction behaviour of CNTAO single crystal. Fig. 12 shows the Arrhenius plot of ac conductivity measured at 300Hz. The ac conductivity (σ) is given by,

$$\sigma = \sigma_0 e^{\frac{-E_{relax.}}{k_B T}} \quad \text{(4)}$$

σ_0 is a constant. The Arrhenius plot (Fig. 12) can be fitted with activation energy of 0.54eV for the low temperature region and 1.05eV for the high temperature. The deviation in Arrhenius equation at higher temperature proves the presence of conduction relaxation in the grown crystal at higher temperatures [7]. The activation energy of 1.05eV proves that the conduction phenomenon is due to the migration of oxygen vacancies at higher temperatures [24]. The Arrhenius plot of ac conductivity for O_2 annealed crystal is shown as inset in Fig. 12, the activation energies for low temperature and high temperature anomalies is 0.56eV and 1.08eV. The increase in activation energy after O_2 annealing from 0.54eV to 0.56eV for low temperature anomaly and 1.05eV to 1.08eV for high temperature anomaly signifies the reduction of oxygen vacancies due to annealing. The calculated activation energies for high temperature region are around 1.05eV which corresponds to the activation energies of doubly ionized oxygen vacancies [11].

Fig. 13 shows the variation of ac conductivity with frequency for different temperatures. It is clearly seen from the plot that dispersion exists in the conductivity values at lower frequencies, but at higher frequencies the curves converge. The deviation in the low frequency region (encircled) is due to the electrode polarization effect [30]. The increase in ac conductivity with frequency can be explained by the charge carriers hopping between Ti^{4+} to Ti^{3+} ions. The resultant increase in conduction process is due to the enhancement of charge carriers hopping with increase in frequency [12, 31]. Mostly in titanates oxygen vacancies play a role as mobile charge carriers, conduction electrons are produced by the ionization of oxygen vacancies which is explained by Kroger-Vink notation as follows [32],

$$O_O^x \longrightarrow \frac{1}{2}O_2 + \ddot{V}_O + 2e^-$$

The oxygen vacancies and excess electron are the products of the reduction reaction. These excess electrons bond with Ti^{4+} following the reaction $Ti^{4+} + e^- \longleftrightarrow Ti^{3+}$ resulting in Ti^{3+} ions. The presence of Ti^{3+} ions was confirmed by X-ray Photoelectron Spectroscopy (XPS) measurements.

The elemental composition and chemical state of the grown crystal is provided by XPS. The full spectrum in Fig. 14 shows that the grown crystal contains Ca, Ti, O, Nd, Al and C elements. The Ti 2p spectrum shown in Fig. 15 was deconvoluted using Gaussian function. The core level binding energy of Ti $2p_{1/2}$ and Ti $2p_{3/2}$ appeared at 463.64eV and 457.97eV respectively with spin orbit coupling of 5.7eV confirm the oxidation state is Ti^{4+}. The difference in binding energy for Ti $2p_{3/2}$ (457.96eV) spectrum and TiO_2 bulk (459.0eV) is of ~1eV suggesting that the presence of Ca affects the ionic character of the Ti-O bond which results in the increase of bond length and hence a decrease in the binding energy as compared with bulk TiO_2 [33,34]. The presence of Ti_2O_3 (Ti^{3+}) at 456.4 eV is being attributed to the presence of oxygen deficiency in the grown crystal [35]. Fig. 16 shows the O1s spectrum which has a well resolved doublet peaks at 529.2 eV and 531.6 eV. The lowest binding energy peak at 529.2 eV is assigned to the oxygen species in the perovskite structure. The higher binding energy peak at 531.6 eV is ascribed to oxygen vacancies [36-40]. The suppression of peak at 531.6 eV after O_2 annealing (shown as inset in Fig. 16) proves the decrease of oxygen vacancies after O_2 annealing treatments. This shows that the grown crystal has oxygen vacancies and these attributes to the dielectric relaxations.

CONCLUSION

Dielectric studies on CNTAO single crystals were done in the temperature range between RT and 660K. Two kinds of dielectric anomalies were observed, the first one occurring at ~436K shows a relaxor-like behaviour, dipolar and Maxwell-Wagner relaxations are the

cause for this anomaly. The activation energies of ~0.4 to 0.5eV for low temperature anomaly prove that these anomalies are due to oxygen vacancies. The annealing treatments in O_2 atmosphere have also proved that these anomalies are dependent of oxygen vacancies. Electrode polarization effect dominates the Maxwell-Wagner relaxations. The formation of Schottky barriers could be the reason for electrode polarization. The higher temperature anomaly occurring at ~520K is a kind of conduction relaxation associated with doubly ionized oxygen vacancies with activation energy of ~1.05eV. The XPS results confirmed the presence of Ti^{3+} ions and presence of oxygen vacancies in the grown single crystal.

Acknowledgements

GM would like to express his gratitude to UGC-DAE Consortium for Scientific Research for providing a financial support and VIT University management for their constant encouragement. This work has been carried out at UGC-DAE Consortium for Scientific Research, Kalpakkam Node, Kokilamedu. GM also thanks Dr. V. Subramanian, Mr. G. Ramesh, Department of Physics, IIT Madras for dielectric measurements, Dr. Fumio Hamada and Dr. Yoshihiko Kondo, Akita University for XPS measurements.

References

1. Rodney C. Ewing, Progress in Nuclear Energy, 49 (2007), 635-643.
2. Bostjan Jancar, Danilo Suvorov, MatjazValant, Goran Drazic, Journal of the European Ceramic Society **23** (2003) 1391–1400.
3. K. Lemanski, A. Gagor, M. Kurnatowska, R. Pazik, P.J. Deren, Journal of Solid State Chemistry **184** (2011) 2713–2718.
4. V.V. Lemanov, A.V. Sotnikov, E.P. Smirnova, M.Weihnacht, R. Kunze, Solid State Commun. **110** (1999) 611–614.
5. V.V. Lemanov, A.V. Sotnikov, E.P. Smirnova, M. Weihnacht, Appl. Phys. Lett. **81** (2002) 886–888.
6. E.R. Kipkoech, F. Azough, R. Freer, C. Leach, S.P. Thompson, C.C. Tang, Journal of the European Ceramic Society **23** (2003) 2677–2682.
7. C. C. Wang, C. M. Lei, G. J. Wang, X. H. Sun, T. Li, J. Appl. Phys. **113** (2013) 094103.
8. L. N. Liu, C. C. Wang, C. M. Lei, T. Li, G. J. Wang, Appl. Phys. Lett. **102** (2013) 112907.

9. Chunchang Wang, Meini Zhang and Wei Xia, J. Am. Ceram. Soc., **96** (2013) 1521–1525.
10. Diouma Kobor, Benoit Guiffard, Laurent Lebrun, Abdelowahed Hajjaji and Daniel Guyomar, J. Phys. D: Appl. Phys. **40** (2007) 2920–2926.
11. Sumit Bhardwaj, Joginder Paul, Subhash Chand, K.K. Raina and Ravi Kumar, J Mater Sci: Mater Electron **25** (2014) 4568–4576.
12. M.R. Shah, A.K.M. Akther Hossain, J. Mater. Sci. Technol., **29** (2013) 323-329.
13. J.L. Ye, C.C. Wang, W. Ni and X.H. Sun, J. of Alloys and Compounds **617** (2014) 850–854.
14. O. Bidault, P. Goux, M. Kchikech, M. Belkaoumi, and M. Maglione, Phys. Rev. B **49** (1994) 7868.
15. G. Murugesan, R. Nithya, S. Kalainathan and T.R. Ravindran, CrystEngComm. **17** (2015) 1982–1988.
16. F.Kremer, A. Schomhals, Broadband Dielectric Spectroscopy, Springer, ISBN: 978-3-642-62809-2.
17. D. O'Neill, R.M. Bowman and J.M. Gregg, Appl. Phys. Lett., **77** (2000) 1520.
18. U. Adem, N. Mufti, A.A. Nugroho, G. Catalan, B. Noheda and T.T.M. Palstra, J. Alloys and Compounds **638** (2015) 228.
19. H. Lu, X. Zhang, B. He and H. Zhang, J. Appl. Polymer Sci., **102** (2006) 3590.
20. S. Sahoo, U. Dash, S.K.S. Parashar and S.M. Ali, J. Advanced Ceramics **2** (2013) 291–300.
21. Shrabanee Sen and R.N.P. Choudhary, Materials Chemistry and Physics **87** (2004) 256–263.
22. W. Li, K. Chen, Y. Y. Yao, J. S. Zhu, and Y. N. Wang, Appl. Phys. Lett. **85** (2004) 4717.
23. X. F. Wang, X. M. Lu, C. Zhang, X. B. Wu, W. Cai, S. Peng, H. F. Bo, Y. Kan, F. Z. Huang and J. S. Zhu, J. Appl. Phys. **107** (2010) 114101.
24. Zhi Yu, Chen Ang, P. M. Vilarinho, P. Q. Mantas, and J. L. Baptista, J. Appl. Phys., **83 (**1998) 4874.
25. Jing Wang, Qiuju Li, Yi Yu, Jian Zhang, Jun Zheng, Chao Cheng, Yide Li, Hong Wang and Chunchang Wang, Physica B **447** (2014) 62–64.
26. A. Baral, K.R.S. Preethi Meher and K.B.R. Varma, Bull. Mater. Sci., **34** (2011) 53.
27. Bondarenko A.S. and Ragoisha G.A. in progress in Chemometrics Research, Pomerantsev A.L.,Ed.; Nova Science Publishers: New York, 2005, pp. 89-102, the program is available online at http://www.abc.chemistry.bsu.by/vi/analyser/
28. Claudia Longo and Marco-A. De Paoli, J. Braz. Chem. Soc. **14** (2003) 889-901
29. C. Longo, A.F. Nogueira and Marco-A.De Paoli. J. Phys. Chem. B **106** (2002) 5925
30. D.K. Pradhan, R.N.P. Choudhary and B.K. Samantaray, Int. J. Electrochem. Sci., **3** (2008) 597
31. S. Sarangi, T. Badapanda, B. Behera and S. Anwar, J Mater Sci: Mater Electron. (2013)
32. F.A. Kroger and H.J. Vink, Solid State Physics **3** (1956) 307.
33. P.V. Nagarkar, P.C. Searson and F.D. Gealy III, J. Appl. Phys., **69** (1991) 459.
34. Y. Mao and S.S. Wong, Adv. Mater. **17** (2005) 2194.
35. K. Bapna, D.M. Phase and R.J. Choudhary, J. Appl. Phys. **110** (2011) 043910.

36. MNaeem, SKHasanain, M Kobayashi, Y Ishida, A Fujimori, Scott Buzby and S Ismat Shah, Nanotechnology 17 (2006) 2675–2680.
37. Adnan Younis, Dewei Chu and Sean Li, J. Phys. D: Appl. Phys. 45 (2012) 355101.
38. Jiayong Gan, Xihong Lu, Jingheng Wu, Shilei Xie, Teng Zhai, Minghao Yu, Zishou Zhang,Yanchao Mao, Shing Chi Ian Wang, Yong Shen & Yexiang Tong, SCIENTIFIC REPORTS | 3 : 1021.
39. P Mohanty, N C Mishra, R J Choudhary, A Banerjee, T Shripathi, N P Lalla, S Annapoorni and Chandana Rath, J. Phys. D: Appl. Phys. 45 (2012) 325301.
40. P.R. Mandal, T.K. Nath, Journal of Alloys and Compounds 628 (2015) 379–389.

Tables and Figures:

Tables:

Table 1. Resulting parameters of the Nqyuist plot fitted to an equivalent circuit described in the text.

Fitted Parameters	Values	Error (%)
R_1	$1 \times 10^6\ \Omega$	4.0098
R_2	31974 Ω	0.13634
CPE (C_1)	9.1253×10^{-7} F	0.13451
n_1	0.388	0.040817
CPE (C_2)	3.581×10^{-11} F	0.68214
n_2	0.978	0.050278

Figures:

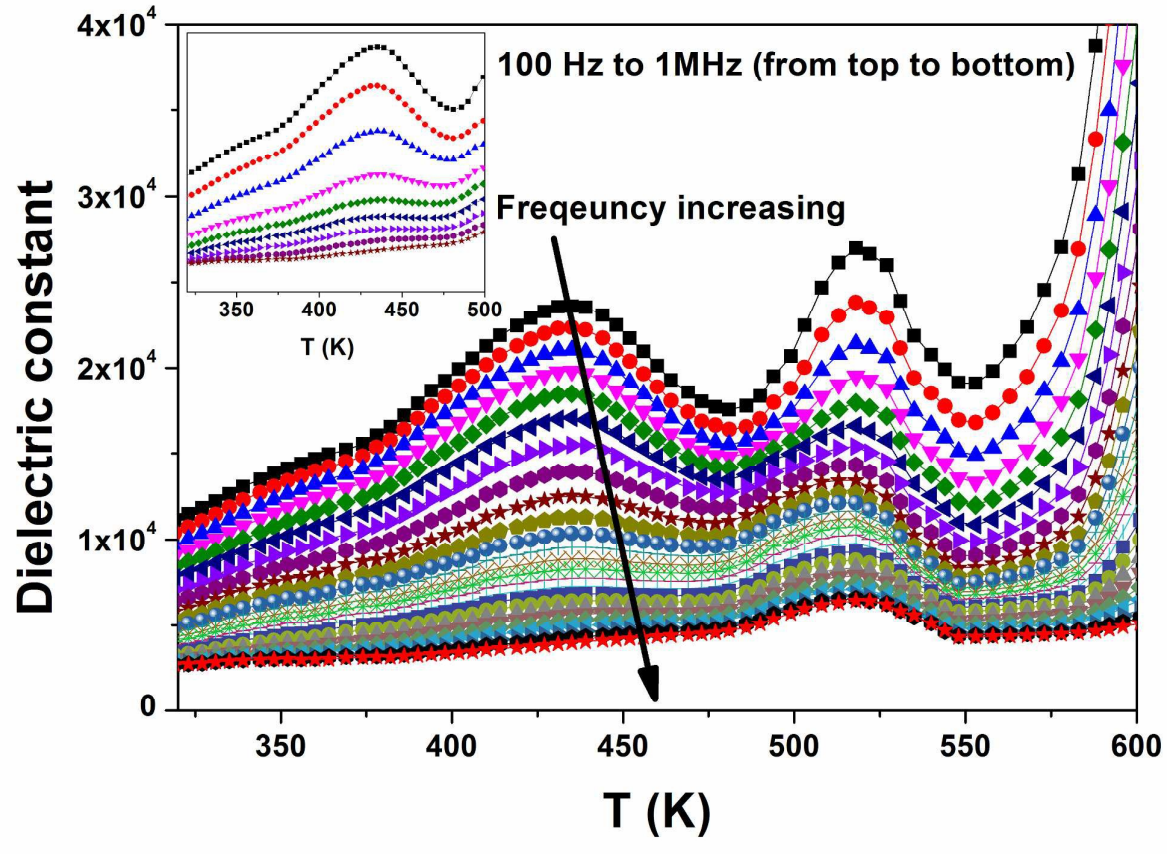

Fig. 1 Temperature dependence of real part of permittivity for CNTAO single crystals measured at various frequencies from 100Hz to 1MHz (from top to bottom). Inset shows the magnified part of the low temperature anomaly.

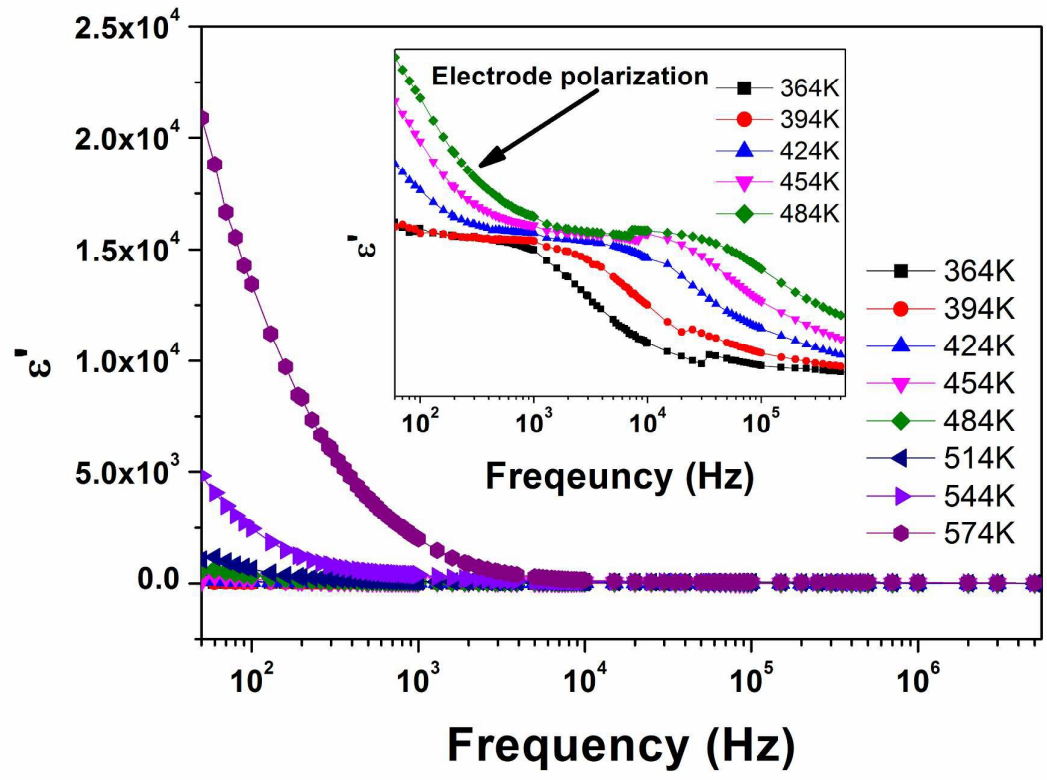

Fig. 2. Dielectric constant as a function of frequency for CNTAO single crystals measured at different frequencies. Inset shows the magnified image of the low temperature region.

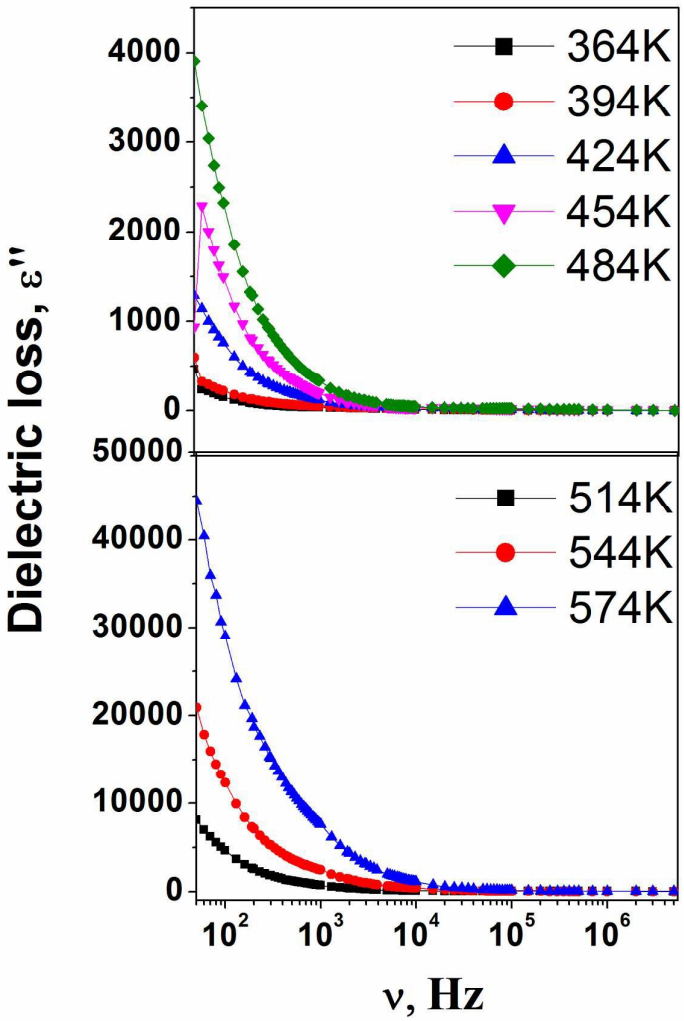

Fig. 3. Dielectric loss as a function of frequency for CNTAO single crystals measured at different frequencies.

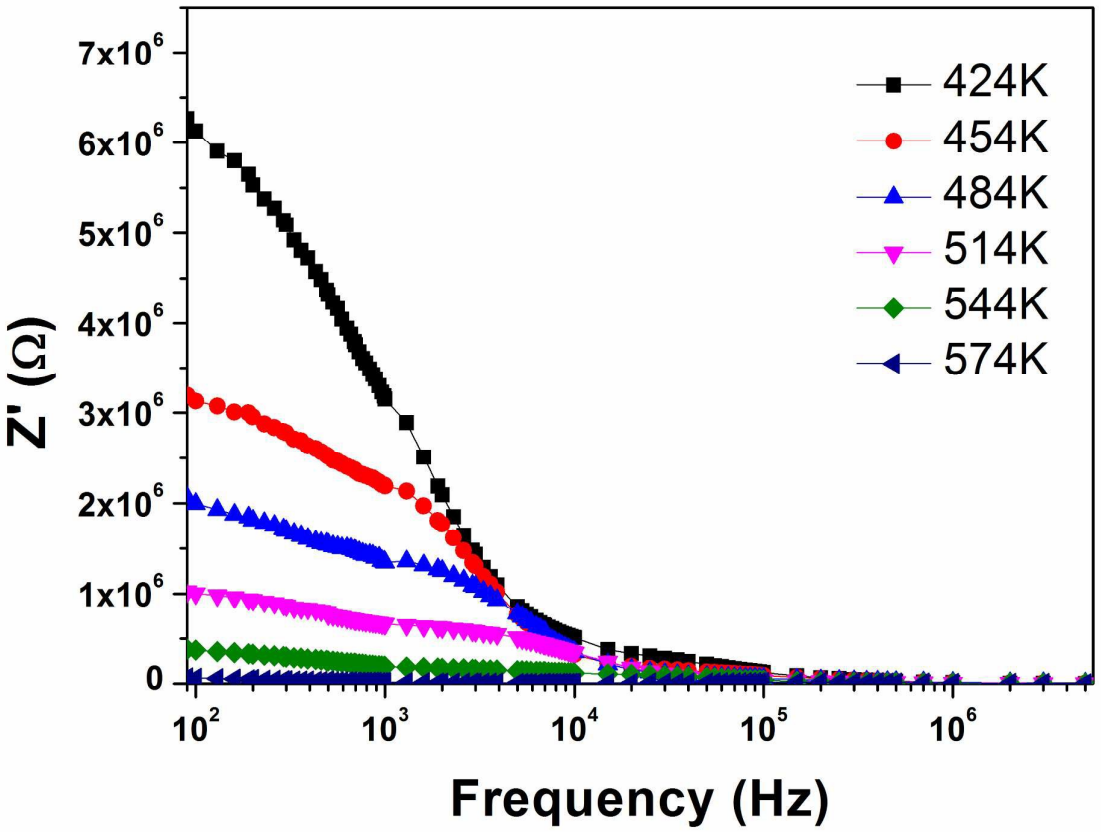

Fig. 4. Frequency dependence of real part Z′ for CNTAO single crystals at various temperatures.

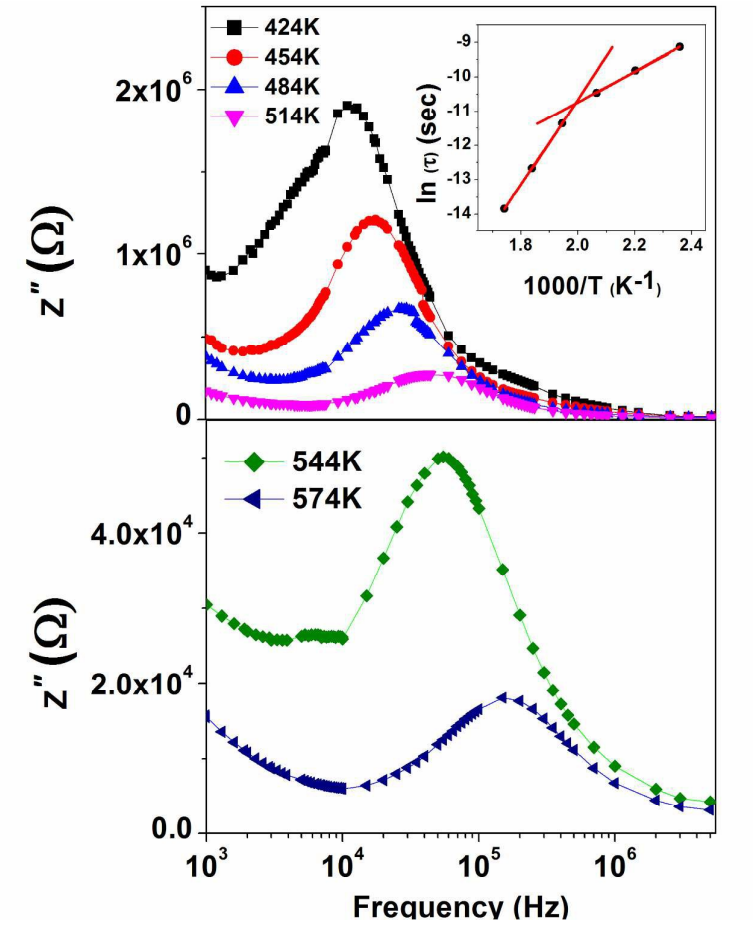

Fig. 5 Frequency dependence of imaginary part Z" for CNTAO single crystals at various temperatures. Inset shows plot of ln(τ) vs 1000/T.

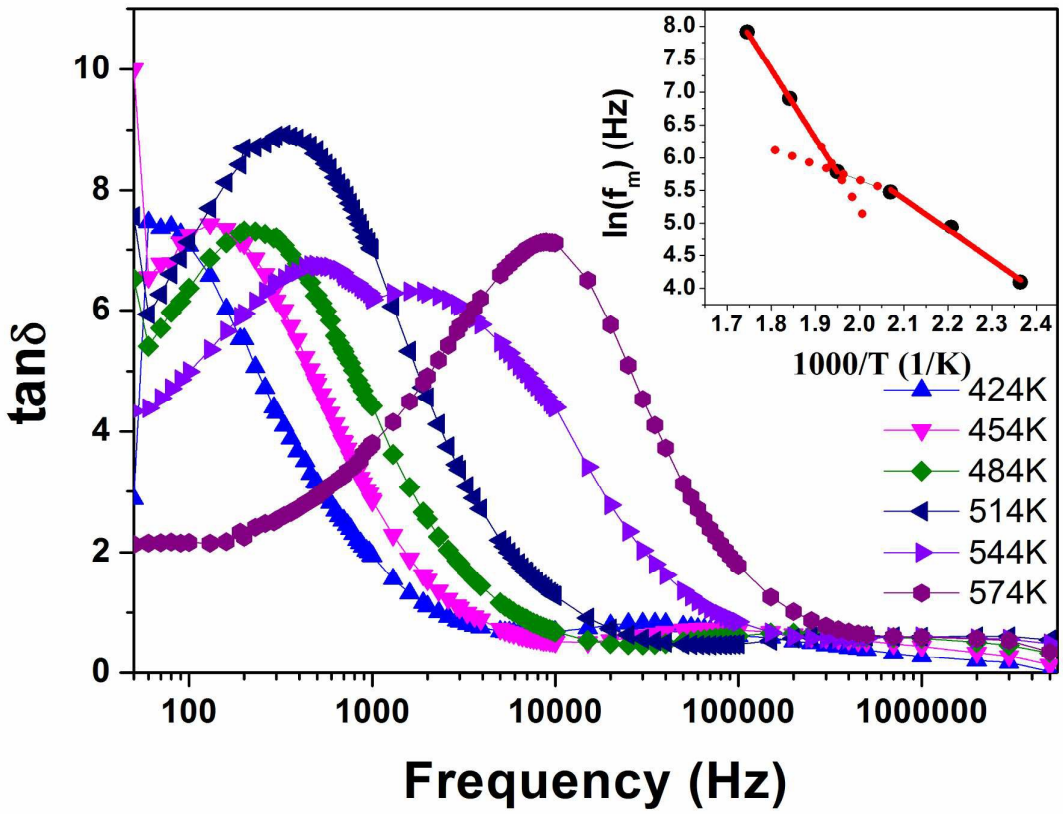

Fig. 6 Frequency dependence of tanδ for CNTAO single crystals at various temperatures. The inset shows the Arrhenius plot of tanδ peak

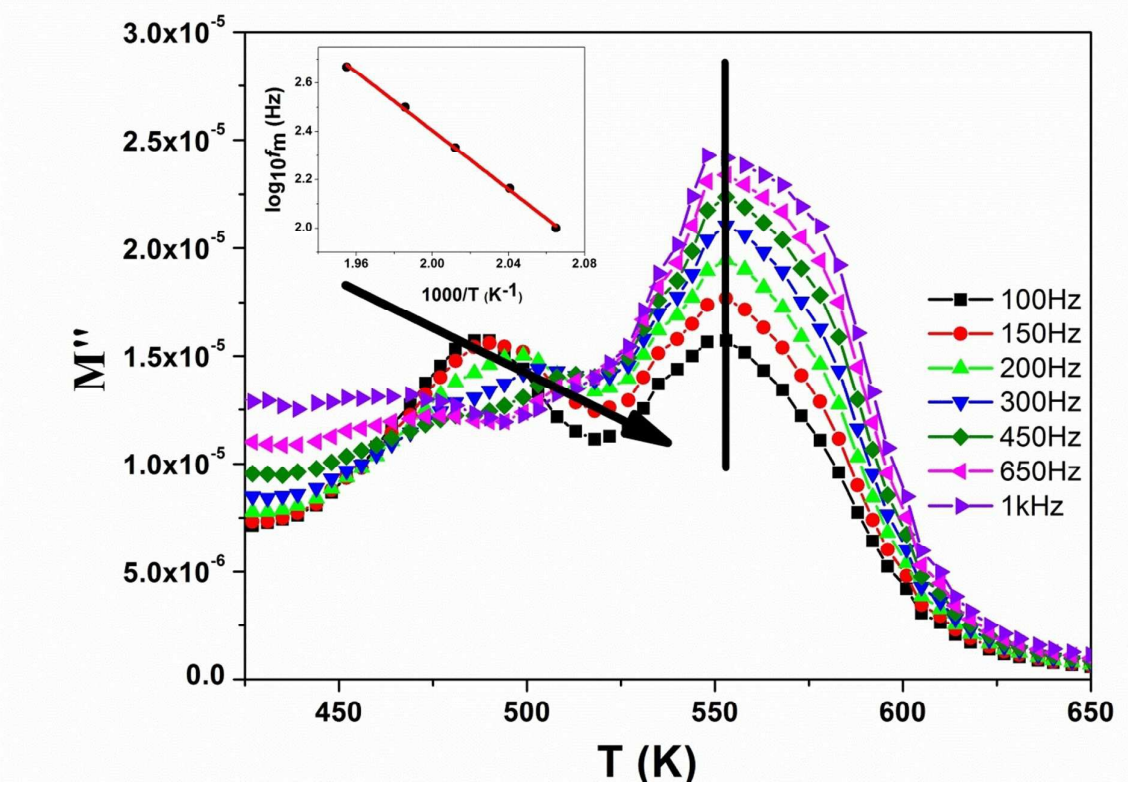

Fig. 7 Temperature dependence of imaginary part of electric modulus for CNTAO crystals at various frequencies. Inset shows the Arrhenius plot of the LT relaxation.

.

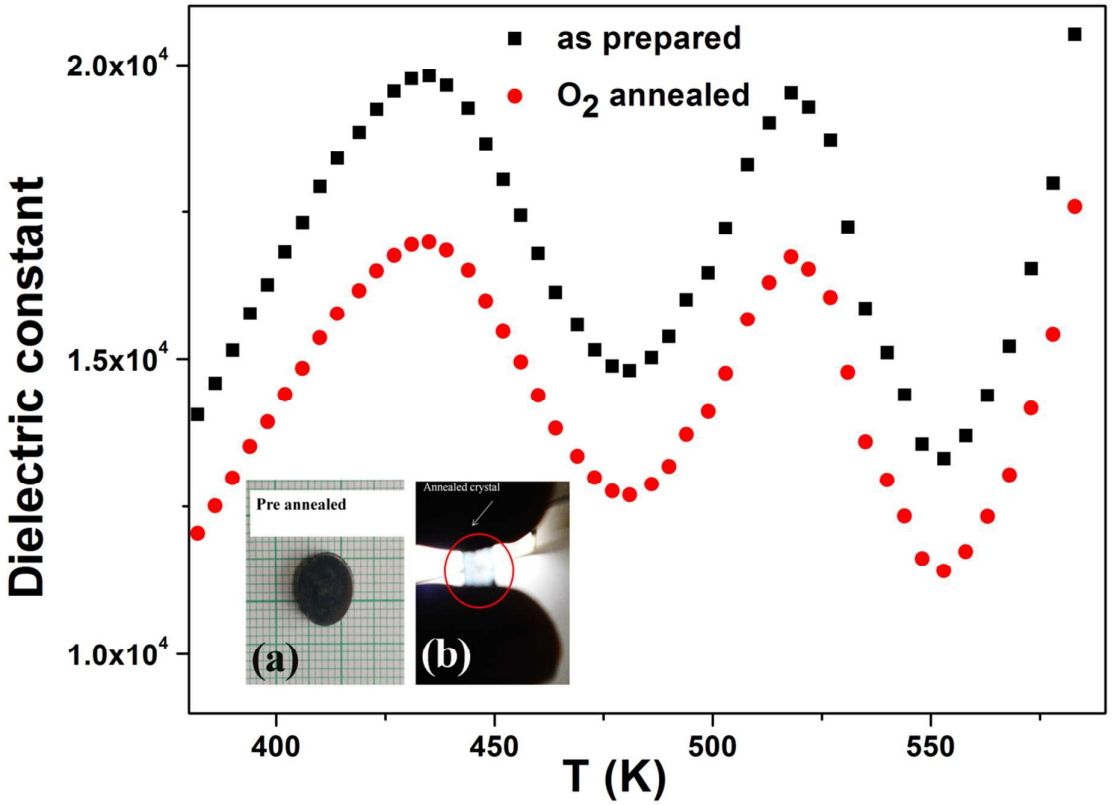

Fig. 8 Temperature dependence of dielectric constant for as prepared and O_2 annealed crystals measured at 300Hz. Inset shows (a) as cut grown crystal before annealing, (b) a part of the crystal after annealing.

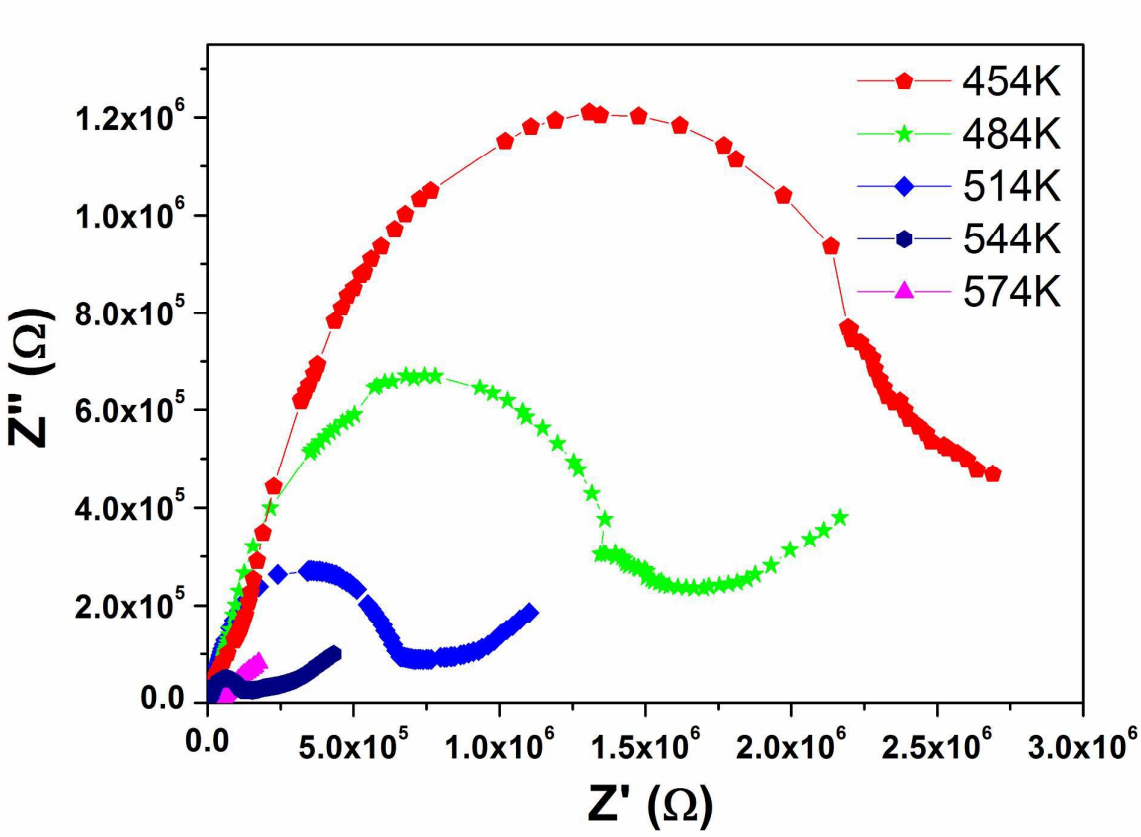

Fig. 9 Nyquist plot for CNTAO single crystals at various temperatures.

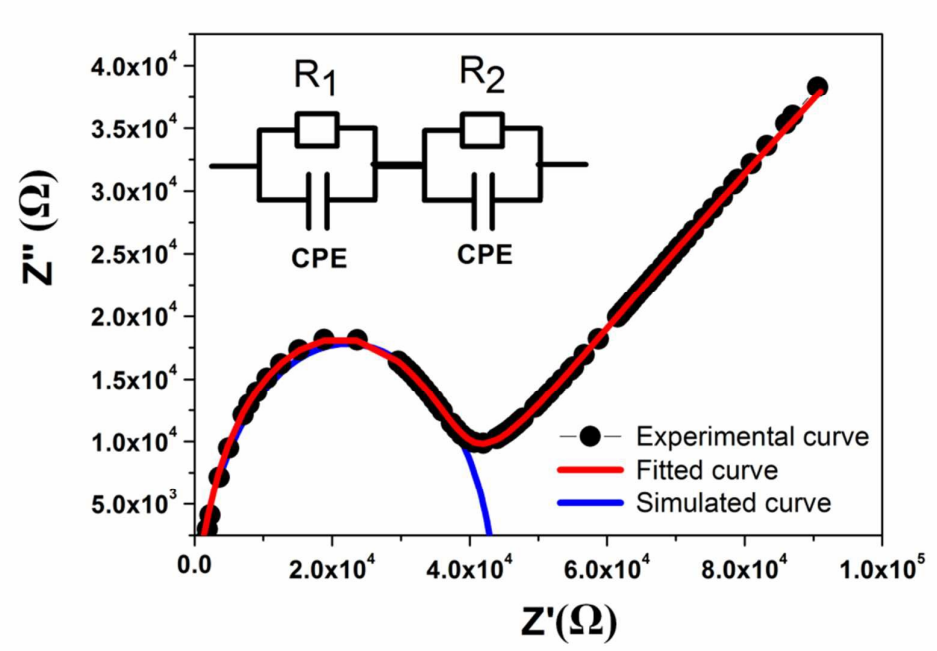

Fig.10 Nyquist plot for CNTAO single crystals at 574K.

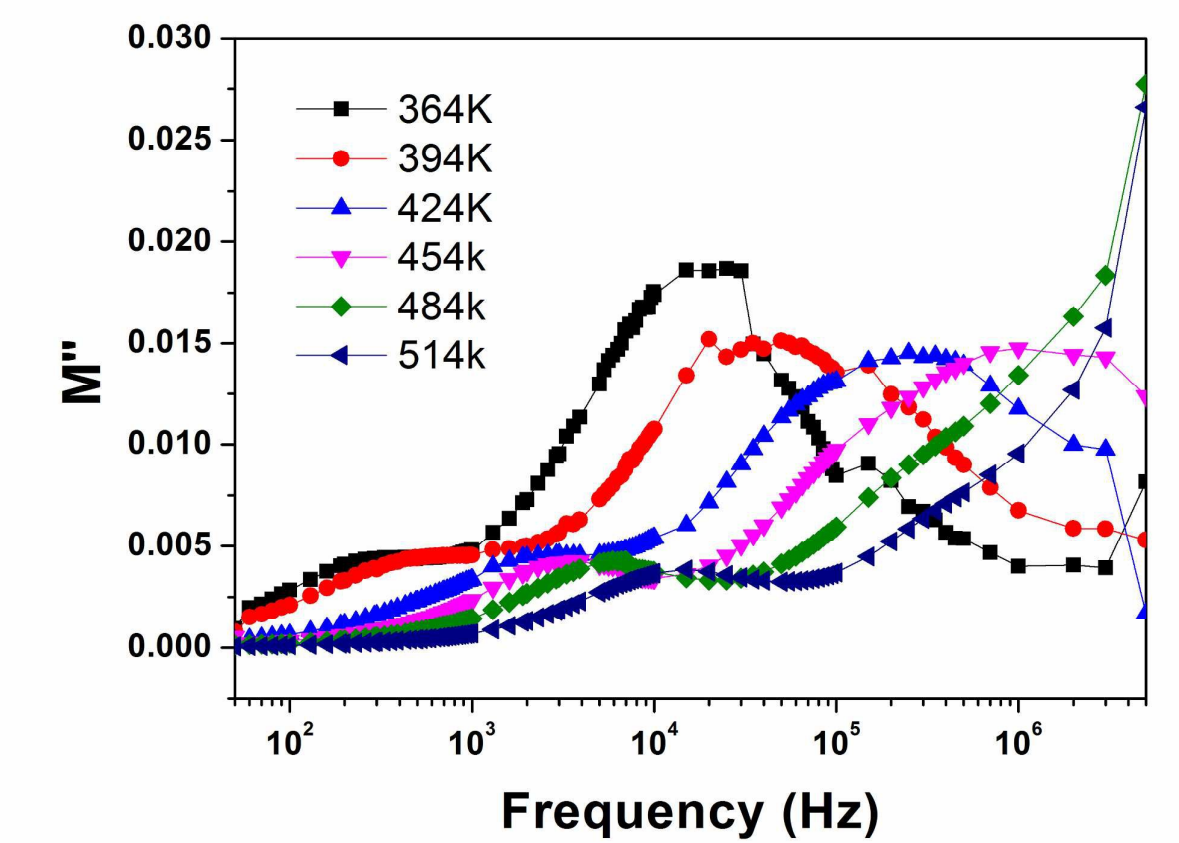

Fig. 11. Frequency dependence of imaginary part M″ for CNTAO single crystals at various temperatures.

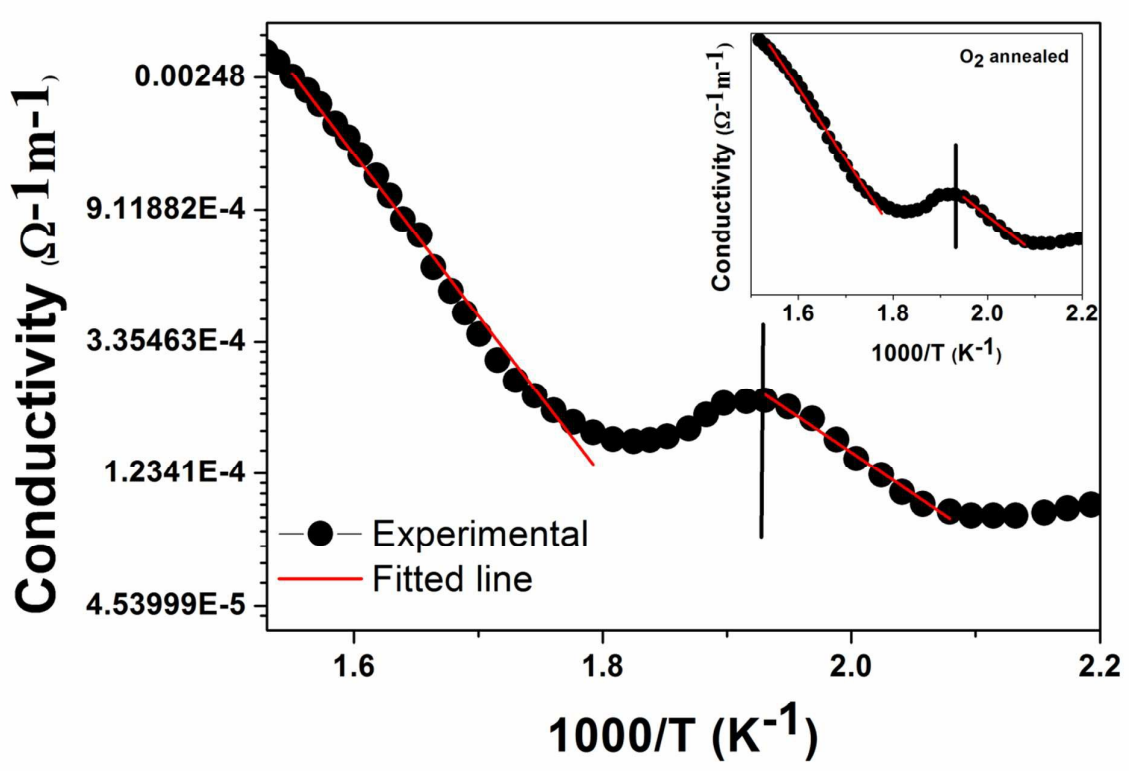

Fig. 12 Temperature dependence of conductivity for the grown CNTAO crystals. Inset shows the temperature dependance of conudcitity for O_2 annealed crystals.

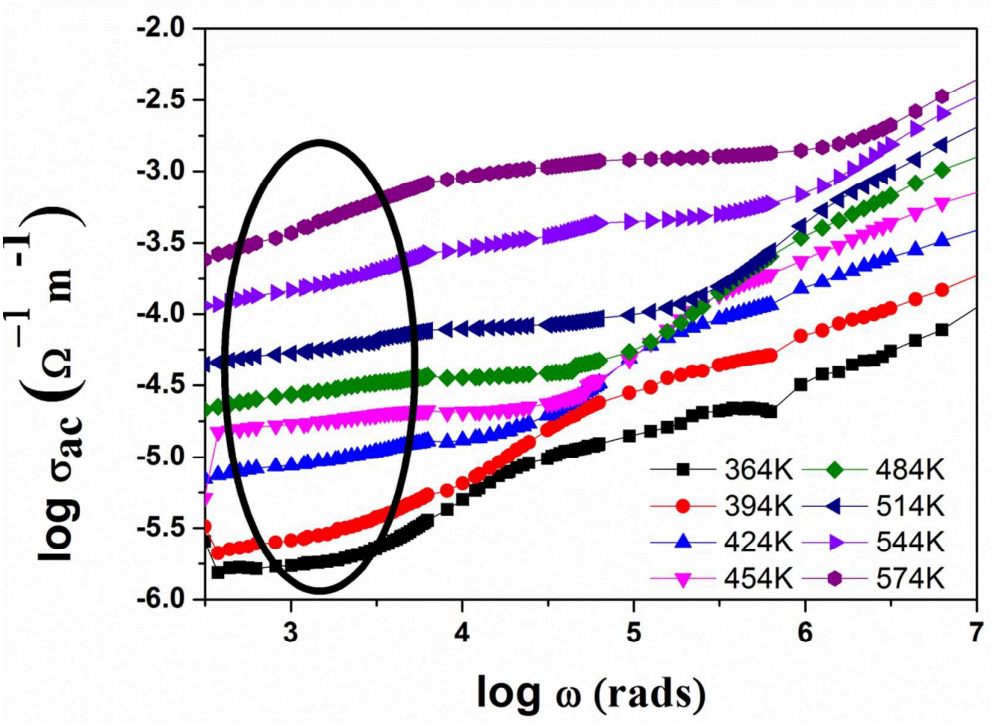

Fig. 13 Frequency dependence of ac conductivity of CNTAO crystals for various temperatures.

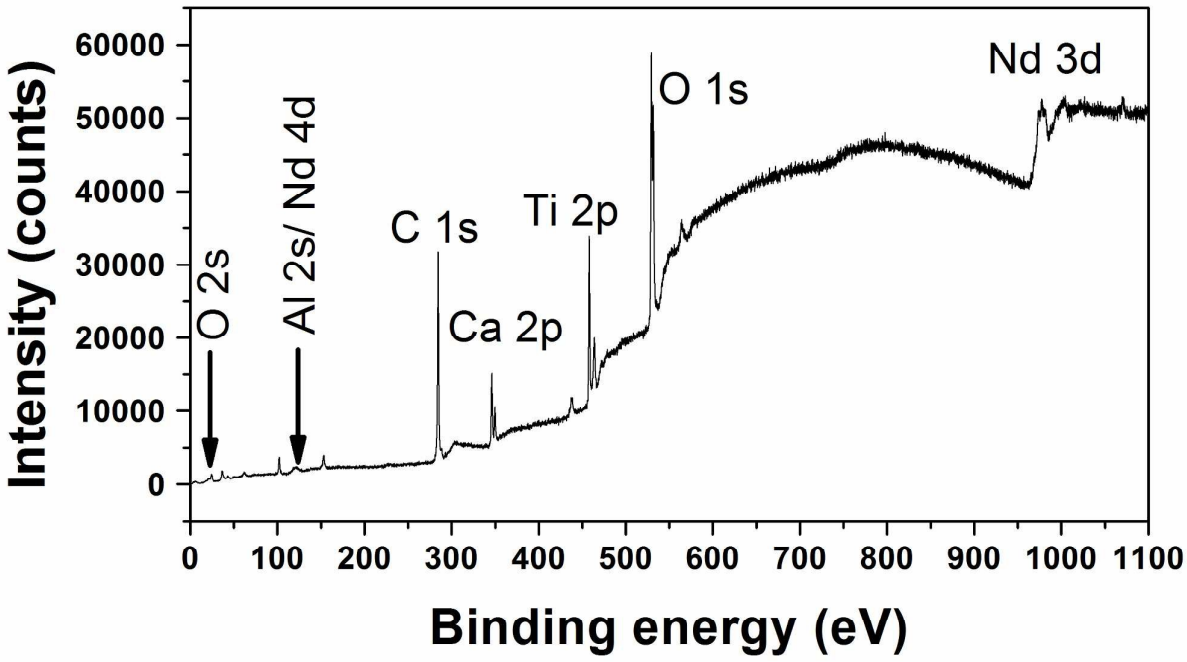

Fig. 14 Wide XPS spectrum of CNTAO single crystals.

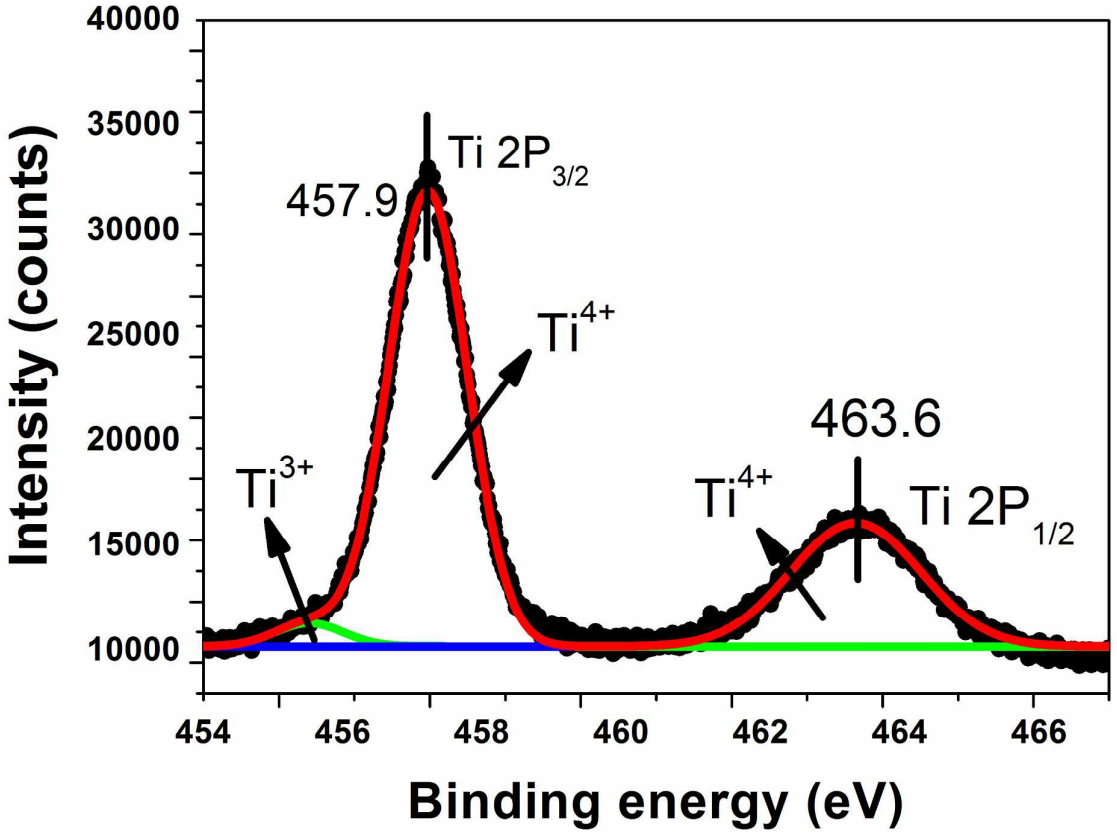

Fig. 15 Ti_{2p} XPS spectrum of CNTAO crystals.

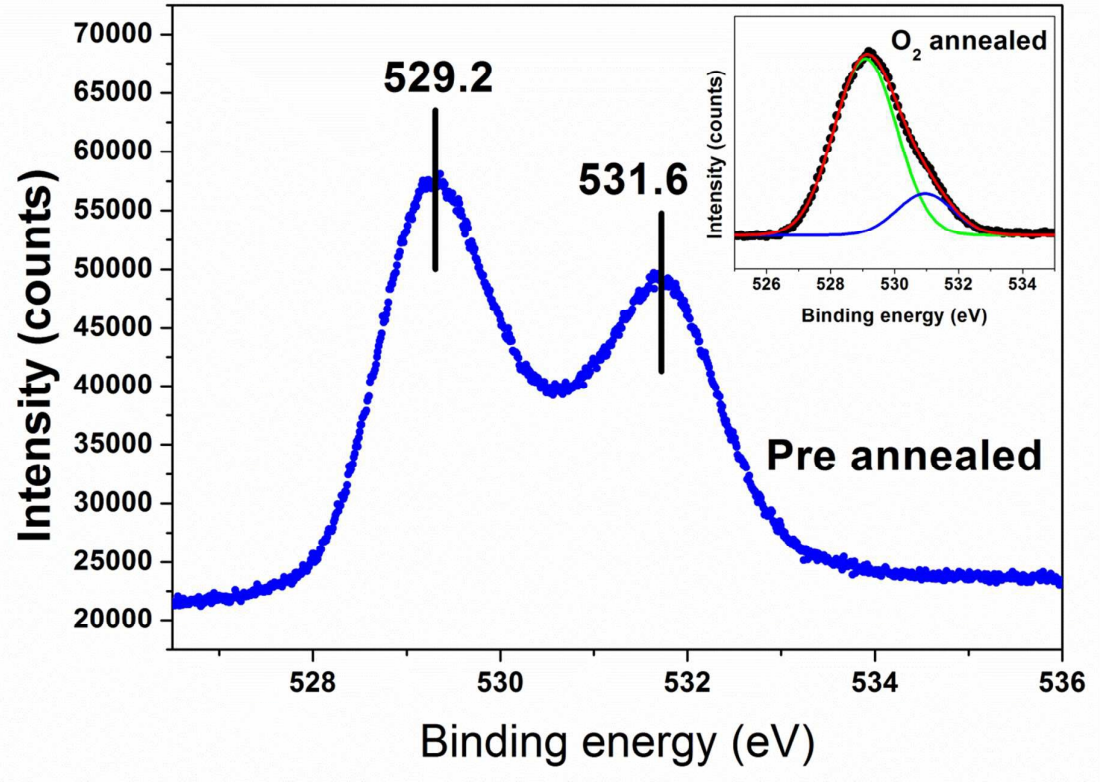

Fig. 16 O1s XPS spectrum of CNTAO crystals, inset shows the O1s spectrum after O_2 annealing